Reports

Convection in a Rotating Layer: A Simple Case of Turbulence

Abstract. *Convection in a layer heated from below and rotating about a vertical axis exhibits a unique phenomenon in fluid dynamics in that the small-amplitude motion is governed by random effects in both its spatial and its time dependence. A simple theoretical description of the phenomenon is compared with laboratory observations. A more detailed mathematical description appears to be feasible because of the weakly nonlinear nature of the problem.*

Considerable progress in the understanding of the onset of turbulence in fluid systems has been achieved in the past decade through studies of the appearance of randomness in simple, well-controlled experiments. Laser Doppler velocimetry measurements of Taylor vortex flow have led to the discovery of discrete transitions to oscillatory, aperiodic, and turbulent flow (*1*), and similar results have been obtained for convection in layers of small aspect ratio (*2*). The sequence of transitions leading to turbulence parallels the behavior of bifurcating solutions of some simple nonlinear systems of ordinary differential equations, of which the Lorenz equations (*3*) are the most famous example. Although the general similarity between the mathematical bifurcation problems and the experimental observations is highly suggestive, a quantitative comparison of theory and measurement has not yet been obtained. The equations describing the experimentally realized fluid motions are partial differential equations and, because of the four-dimensional nature of the mathematical problem, it is difficult to derive accurate models of the observed phenomena.

Our purpose in this report is to point out a particularly simple example of the transition to turbulence for which a close correspondence with the solutions of a system of three ordinary differential equations does exist. The phenomenon of convection in a layer heated from below and rotating about a vertical axis has been studied before (*4*), but only recently have sufficiently detailed observations of the time dependence of the convection cells been made (*5*) to permit a comparison with the theoretical predictions (*6, 7*). Before discussing some of the experimental observations, we will briefly consider the theoretical problem.

A horizontal layer of fluid of thickness d is heated from below and rotating about a vertical axis with the angular velocity Ω. It is assumed that the centrifugal force is negligible in comparison with gravity so that the physical conditions are homogeneous and isotropic with respect to the horizontal dimensions and a static state exists as a basic solution of the problem. The temperatures T_2 and T_1 at the lower and upper boundaries are fixed. For the velocity field either a no-slip or a stress-free condition may be applied at the boundaries. By using d, $T_2 - T_1$, and d^2/κ as scales for length, temperature, and time, respectively, the physical conditions of the layer can be represented in terms of the dimensionless parameters Rayleigh number,

$$R = \gamma(T_2 - T_1)gd^3/\kappa\nu$$

Taylor number,

$$T = 4\Omega^2 d^2/\nu^2$$

and Prandtl number,

$$P = \nu/\kappa$$

where κ is the thermal diffusivity, ν is the kinematic viscosity, γ is the coefficient of thermal expansion, and g is the acceleration due to gravity. When the Rayleigh number exceeds a critical value R_c depending on the Taylor number T the static state becomes unstable and convective motions set in (*8*). The linear analysis describing the onset of convection predicts the horizontal wave number α_c of the motions but does not determine their horizontal structure. A general description of the latter is given by the following expression for the vertical component of the velocity field in the limit of small amplitudes

$$u_x^{(0)} = f(z, \alpha_c) \sum_{n=-N}^{N} c_n \exp\{i\mathbf{k}_n \cdot \mathbf{r}\} \quad (1)$$

where z is the component of the position vector $\mathbf{r}$ in the vertical direction and the horizontal vectors $\mathbf{k}_n$ are arbitrary except for the conditions

$$|\mathbf{k}_n| = \alpha_c, \mathbf{k}_{-n} = -\mathbf{k}_n \text{ for } n = 1, \cdots, N$$

The coefficients c_n represent arbitrary complex numbers subject to the conditions

$$c_n = -c_n^+$$

where c_n^+ denotes the complex conjugate of c_n. The parameter N indicating the number of nonvanishing coefficients c_n may vary from one to infinity.

In order to decide which solution among the manifold of Eq. 1 is physically realized, the nonlinear equations must be considered. By using a perturbation approach for the weakly nonlinear problem, it was found in the case $T = 0$ that only solutions corresponding to $N = 1$ and describing convection in the form of two-dimensional rolls are stable with respect to arbitrary infinitesimal disturbances (*9*). Küppers and Lortz (*6, 10*) extended this result to the case of finite values of T. In addition, they found that all solutions including rolls are unstable when T exceeds a critical value T_c, which depends slightly on the Prandtl number and assumes the value 2285 for $P = \infty$ in the case of stress-free boundaries. For a given roll solution described by the wave vector $\mathbf{k}_1$ the instability assumes the form of secondary rolls characterized by the vector $\mathbf{k}_2$, which encloses an angle ϕ with $\mathbf{k}_1$. The angle ϕ has a value of about 58° when measured in the direction of rotation and varies little with the Prandtl number.

To answer the question of what form of convection is physically realized, the initial value problem must be considered. Since the instability develops on the time scale $(R - R_c)d^2/R_c\kappa$, it is sufficient to consider weakly time-dependent solutions of the form of Eq. 1 with coefficients c_n that are now assumed to depend on time. Starting with the initial value for c_1 given by the steady solution for two-dimensional rolls and much smaller values for all other coefficients c_n, the integration exhibits the instability predicted by Küppers and Lortz when T exceeds T_c. The coefficient c_2 corre-

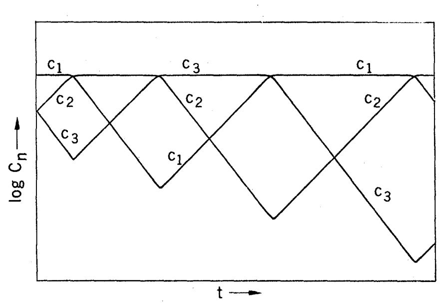

Fig. 1. Time dependence of the coefficients c_n. Because the amplitudes y_n are proportional to c_n^2, the solutions of Eqs. 2 exhibit the same behavior.

0036-8075/80/0411-0173$00.50/0

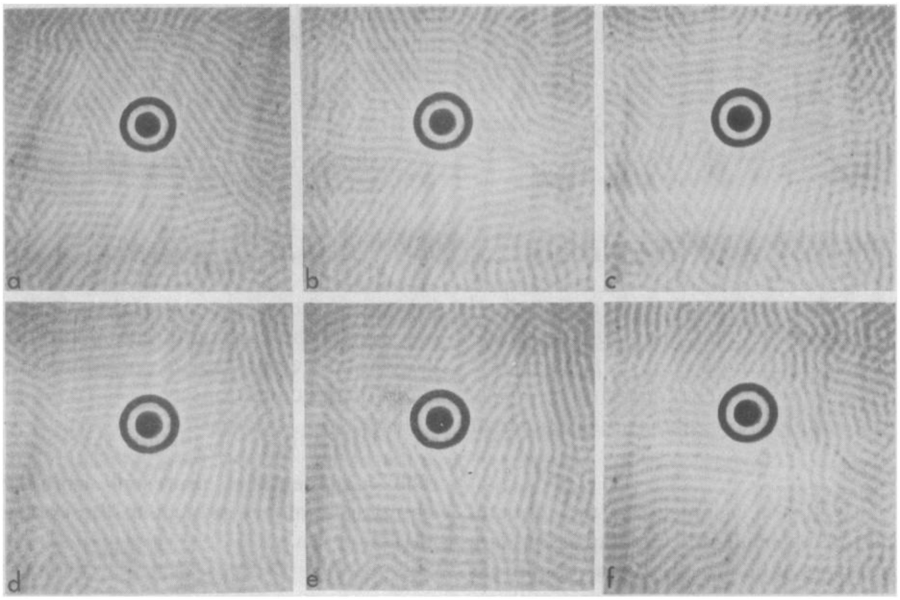

Fig. 2. Development in time of the horizontal structure of convection in a rotating layer heated from below. The parameters of the experiments are $\Omega = 1.29\ \text{sec}^{-1}$, $d = 3.3 \times 10^{-3}$ m, and $R = 3.8 \times 10^3$. The fluid is methyl alcohol ($\nu = 7 \times 10^{-3}\ \text{cm}^2/\text{sec}$ and $\kappa = 1.0 \times 10^{-3}\ \text{cm}^2/\text{sec}$). The number of revolutions since the start of the experiment is 1208, 1348, 1488, 1628, 1716, and 1945 for (a) to (f), respectively.

sponding to the vector $\mathbf{k}_2$, which approximately encloses the angle ϕ with $\mathbf{k}_1$, grows until it reaches an amplitude comparable to that of c_1, at which point c_1 starts to decay and c_2 replaces c_1 as the approximately steady solution. At the same time, the disturbance amplitude c_3 corresponding to the vector $\mathbf{k}_3$, which encloses an angle close to ϕ with $\mathbf{k}_2$, starts growing exponentially and eventually replaces c_2, as shown in Fig. 1. Since c_3 had been decaying before it started growing, it takes longer for the disturbances to reach the equilibrium value. Since ϕ is close to 60°, a simple model is obtained by restricting the analysis to the case $N = 3$ and assuming an angle of exactly 60° enclosed by neighboring vectors $\mathbf{k}_n$. In this case the process repeats itself cyclically as shown in Fig. 1. After suitable renormalization, the equations for the amplitudes $y_n \equiv |c_n|^2$ can be written in the form

$$\begin{aligned} \dot{y}_1 &= (1 - y_1 - \beta y_2 - \gamma y_3)y_1 \\ \dot{y}_2 &= (1 - y_2 - \beta y_3 - \gamma y_1)y_2 \qquad (2) \\ \dot{y}_3 &= (1 - y_3 - \beta y_1 - \gamma y_2)y_3 \end{aligned}$$

where the dot denotes differentiation with respect to time. System 2 is identical to a system of equations considered in population biology (*11*). For $T > T_c$, $^1/_2(\beta + \gamma)$ exceeds unity and all equilibrium points of Eqs. 2 are unstable, leading to the behavior exhibited in Fig. 1. A nonphysical feature of this solution is that the properties of the system depend on the time elapsed since the initial conditions were set. The resolution of this paradoxical result comes from the recognition that in any fluid system, small-amplitude disturbances are present at all times and not just at the initial moment, as assumed in the solution shown in Fig. 1. The existence of a noise level prevents the amplitudes y_n from decaying to arbitrary small levels. At the same time it introduces a random element into the time dependence of the system; that is, the system acquires one of the characteristic properties of turbulent fluid flow. Accordingly, it must be expected that the cycles displayed in Fig. 1 become nearly periodic, but with a period that fluctuates statistically in time.

The experimental observations confirm this theoretical picture at any particular point in the convection layer. But the problem is complicated by the fact that randomness develops in the spatial dependence, as well as in the time dependence. Even if a convection pattern in the form of two-dimensional rolls is generated by controlled initial conditions, the changeover from the unstable roll pattern described by c_1 to the roll pattern described by c_2 is completed at different times in different places because of the statistical spatial variations of the disturbance amplitudes. The fractionation of the convection pattern into patches of rolls with different orientation is balanced by the effects of horizontal diffusion. Thus the average size of a patch of approximately homogeneous rolls depends inversely on the growth rate of the instability, which is proportional to the deviations of both the Rayleigh number and the Taylor number from their critical values.

Figure 2 shows a typical sequence of pictures of the horizontal structure of convection under stationary conditions. The photographs were obtained by the shadowgraph visualization method (*12*). A parallel beam of light traverses the layer and experiences slight deflections because of the variation with temperature of the index of refraction of the convecting fluid. Accordingly, dark and light areas in the pictures indicate hot rising and cold descending fluid, respectively. The circular feature near the center of each picture is a part of the apparatus that does not interfere with the formation of the pattern.

The sequence of pictures in Fig. 2 shows that convection rolls at a particular place are replaced as time goes on by new convection rolls inclined at an angle of about 60° in the counterclockwise direction with respect to the old rolls. In the case of the patch of rolls on the lower left side, the sequence of instabilities completes a full cycle and the patch of rolls in Fig. 2f looks surprisingly similar to that in Fig. 2a. The instability usually progresses from a neighboring patch with rolls of suitable orientation. The theoretical scenario outlined above does not take into account this aspect and a more detailed theory is required to represent the nonlocal properties of the process. Since the equations describing the convection are only weakly nonlinear, a comprehensive two-scale analysis is feasible based on the difference between the size of the patches and the wavelength of the rolls.

Even the simple system of Eq. 2 is quite accurate in describing the local evolution in time of the convection pattern if an appropriate lower bound for the amplitude of the disturbances is introduced. A quantitative comparison on this basis will not be attempted here. The experimental observations shown in Fig. 2 clearly indicate that the particularly simple case of turbulence in a rotating convection layer can be understood in terms of a manifold of stationary solutions, each of which is unstable with respect to another solution of the same manifold so that the system evolves in time by realizing cyclically the different solutions of the manifold. It will be of interest to see the extent to which this concept applies to more complex turbulent fluid systems.

F. H. Busse

K. E. Heikes

Department of Earth and Space Sciences, University of California, Los Angeles 90024

References and Notes

1. J. P. Gollub and H. L. Swinney, *Phys. Rev. Lett.* **35**, 927 (1975).
2. J. P. Gollub, S. L. Hulbert, G. M. Dolny, H. L. Swinney, in *Photon Correlation Spectroscopy and Velocimetry*, H. Z. Cumming and E. R. Pike, Eds. (Plenum, New York, 1977), pp. 425–439.
3. E. N. Lorenz, *J. Atmos. Sci.* **20**, 130 (1963).
4. E. L. Koschmieder, *Beitr. Phys. Atmos.* **40**, 216 (1967); H. T. Rossby, *J. Fluid Mech.* **36**, 309 (1969); R. Krishnamurti, in *8th Symposium on Naval Hydrodynamics* (Rep. ARC-179, Office of Naval Research, Washington, D.C., 1971), pp. 289–310.
5. K. E. Heikes, thesis, University of California, Los Angeles (1979).
6. G. Küppers and D. Lortz, *J. Fluid Mech.* **35**, 609 (1969).
7. F. H. Busse and R. M. Clever, in *Recent Developments in Theoretical and Experimental Fluid Mechanics: Compressible and Incompressible Flows*, U. Müller, K. G. Roesner, B. Schmidt, Eds. (Springer-Verlag, New York, 1979), pp. 376–385.
8. S. Chandrasekhar, *Hydrodynamic and Hydromagnetic Stability* (Clarendon, Oxford, 1961).
9. A. Schlüter, D. Lortz, F. H. Busse, *J. Fluid Mech.* **23**, 129 (1965).
10. G. Küppers, *Phys. Lett. A* **32**, 7 (1970).
11. The mathematical properties of the system of Eqs. 2 have been discussed by R. M. May and W. J. Leonard [*J. Appl. Math.* **29**, 243 (1975)]. We are indebted to L. N. Howard for pointing out this reference to us.
12. The shadowgraph method was first applied by M. M. Chen and J. A. Whitehead [*J. Fluid Mech.* **31**, 1 (1968)] for the visualization of convection patterns. For further details, see F. H. Busse and J. A. Whitehead [*J. Fluid Mech.* **47**, 305 (1971)].
13. Support of the research under NSF grant ATM 76-22280 is gratefully acknowledged.

26 November 1979

Evolutionary Implications of Pliocene Hominid Footprints

Abstract. *Hominid footprints discovered at the Pliocene (3.6 to 3.8 million years ago) site of Laetoli in northern Tanzania represent the earliest evidence of bipedalism in human evolution. This new evidence emphasizes the mosaic pattern of human evolution.*

The site of Laetoli in northern Tanzania (3°12′S, 35°11′E) has yielded abundant fossils of Pliocene age. Included among the 5000 vertebrate specimens recovered from Laetoli are remains of 24 hominid individuals (*1*). The Laetolil Beds include a laminated airfall tuff (Tuff 7) that bears the tracks of Pliocene animals ranging in size from millipedes to large elephantids (*2*). Vertebrate fossils and tracks from the Laetolil Beds are radiometrically dated to between 3.6 and 3.8 million years (*1*).

Hominid footprints were discovered at Laetoli site G by Dr. Paul Abell in July of 1978. Illustrations and descriptions of the discoveries are available (*2*). The footprints are undoubtedly in situ and as old as reported.

Excavations at site G in 1978 and 1979 revealed trails of at least two hominid individuals. Portions of the trails are eroded but several intact prints are preserved. The uneroded footprints show a total morphological pattern like that seen in modern humans. Heel strike is pronounced. The great toes appear fully adducted, lying immediately ahead of the ball of the foot. The medial longitudinal arch of the foot is well developed. Spatial relationships of the footprints are strikingly human in pattern. Preliminary observations and experiments suggest that the Laetoli hominid trails at site G do not differ substantially from modern human trails made on a similar substrate.

Discoveries of fossilized hominid remains at Hadar in Ethiopia (2.6 to 3.3 million years ago) (*3*) and Laetoli in Tanzania (3.6 to 3.8 million years ago) (*1*) provide a new perspective on hominid evolution during Pliocene and Pleistocene times. These sites provide the earliest skeletal evidence of the Hominidae. The fossil material is assigned to *Australopithecus afarensis* (*4*), the only hominid species known from rocks of this age.

Numerous investigators have estimated stature in early hominids by using skeletal remains (*5, 6*). The Laetoli footprints can be used in a similar manner, but stature estimates derived from footprint dimensions are based on numerous assumptions. If it is assumed that (i) Laetoli hominids had foot proportions like modern humans, (ii) the individuals represented were adult, (iii) the footprints are good indicators of foot length, and (iv) the reported measurements are accurate; then stature estimates are as given in Table 1 (*7*). These estimates are consistent with those derived from the postcranial skeleton of *A. afarensis*. All available evidence makes it probable that the Laetoli hominid footprints were made by members of this Pliocene species.

Table 1. Stature reconstruction. Stature estimates for the two Laetoli individuals are given here. These estimates are based on average values for modern human populations and are based on several assumptions; M, male; F, female.

Human (*7*)	Foot-length average (%)*	Stature estimates (meters) (*2*) of Laetoli hominids	
		Larger†	Smaller‡
Bushmen (San)	M 14.6	1.47	1.27
	F 14.4	1.49	1.29
Mawambi Pygmy	M 15.6	1.38	1.19
	F 15.5	1.39	1.18
Japanese	M 13.8	1.56	1.34
	F 14.9	1.44	1.24
American Negro	M 15.9	1.35	1.16
	F 16.1	1.34	1.15
American White	M 15.0	1.43	1.23
	F 14.0	1.54	1.32

*Percentage of body height. †Footprint length, 21.5 cm. ‡Footprint length, 18.5 cm.

The acquisition of erect posture and striding bipedal gait by human ancestors represented a major evolutionary event. Anatomical correlates of this form of stature and locomotion have been the subjects of many comparative studies (*8–11*). Anthropologists and zoologists define the family Hominidae on the basis of anatomical features associated with habitual bipedal locomotion (*9, 10, 12–14*).

Students of human evolution have speculated freely on the origins of bipedal locomotion. They have suggested that the protohominid involved in the transition to habitual striding bipedalism was like the gibbon (*15*), the pygmy chimpanzee (*16*), or even *Gigantopithecus* (*17*). Selective factors posited to account for this transition have included vision over tall grass, carrying food or offspring, eating seeds, intimidating rivals or predators (or both), and using tools (*18*).

In the absence of fossil evidence, scholars were forced to speculate on the evolution of structures like the human foot by relying on comparative anatomy and embryology (*14, 19, 20*). Calling on Darwinian gradualism and a *scala naturae* of modern primates, most comparative anatomists predicted that, when fossil hominids were found, they would show various stages of intermediacy between modern humans and chimpanzees (*21*). Early interpretations of Neanderthals and *Homo erectus* were undoubtedly influenced by such reasoning, and hence many reconstructions were depicted with semidivergent great toes (*22*). There has been a persistent reluctance on the part of human paleontologists to acknowledge fossil hominid postcranial remains as indicative of a fully modern human gait (*23*). When information on the skeletal anatomy of *Australopithecus* was gathered in the Transvaal, it was recognized that these fossils were very old (*24*) and anatomically distinct from modern humans in their crania (*11, 25, 26*), shoulder girdles (*27*), arms (*28*), hands (*29*), pelves (*11, 13, 30–34*), femora (*34–36*), ankles (*20, 26, 37*), and limb proportions (*38*).

The significance of these differences

0036-8075/80/0411-0175$00.50/0